Comparative Analysis on the Stability Mechanism of Droop Control and VID Control in DC Microgrid*

Gang Lin[1], *Wei Zuo*[2], *Yong Li*[2*], *Jiayan Liu*[1], *Shaoyang Wang*[2] *and Pengcheng Wang*[3]
(1. Institute of Energy Systems, Energy Efficiency and Energy Economics, TU Dortmund University, Dortmund 44227, Germany;
2. College of Electrical and Information Engineering, Hunan University, Changsha 410082, China;
3. College of Electrical Engineering, Zhejiang University, Hangzhou 310027, China)

Abstract: Voltage resonance and fluctuation deteriorate the stability of DC microgrids (DC-MGs) and restrict their popularization. Conventional droop control cannot suppress voltage fluctuation and damp oscillations. Therefore, new control methods, namely, droop+filter control and virtual inertia and damping control, are proposed. These methods differ owing to the addition of low pass filter (LPF) and virtual inertia loop. In this study, the stability of these control methods is investigated comprehensively to understand their differences arising from the use of LPF and inertia loop as well as the underlying dynamic stability mechanism. The leading causes of voltage instability in DC-MGs regulated by droop control are first presented. Subsequently, control methods for solving this issue are compared and their simplified small-signal models are constructed. Based on eigenvalue analysis, the DC-MG is equivalent to a third-order system. Different control effects can be acquired by changing the control parameters and the location of the eigenvalues; furthermore, they can be used to understand the dynamic stability. Eigenvalue analysis can provide parameter design guidelines. Finally, the simulation results verify the validity of the theoretical analysis.

Keywords: DC microgrid, dynamic characteristic, virtual inertia, small-signal model

1 Introduction

The energy crisis and environmental issues have promoted the widespread application of distributed generations (DGs). Renewable energy sources, such as photovoltaics (PV) and wind energy have developed rapidly in recent decades [1-2]. The advantages of high efficiency and wide application of DC loads render DC microgrids (DC-MGs) the main target for DGs. Furthermore, DC-MGs will become the main power supply architecture for certain applications in the future, such as smart buildings, power electronic loads, and ships [3]. A typical DC-MG configuration diagram is shown in Fig. 1. During a grid-connected operation, the utility grid stabilizes the bus voltage. When DC-MGs operate in isolation, DGs supply the power, whereas the energy storage system (ESS) balances the power deviation and maintains the DC bus voltage stability. Various DGs, ESSs, and loads are connected to the DC bus via fast-response converters, rendering the DC-MG a poor damping and low-inertia power system. When a DC-MG is disturbed, resonance, voltage fluctuation, and oscillation will occur easily, thereby hindering the application of DC-MGs [4-5].

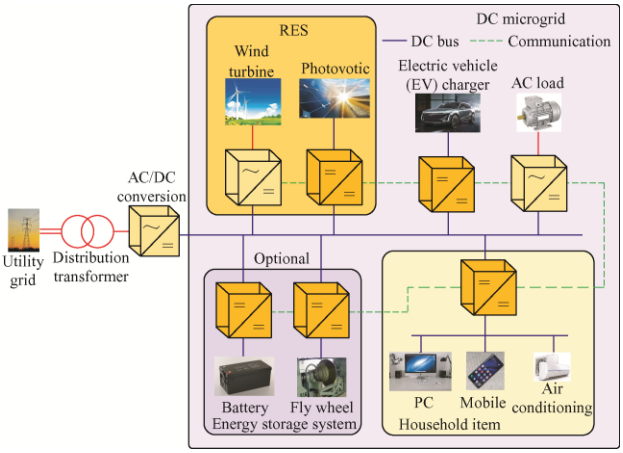

Fig. 1 Diagram illustrating typical DC-MG configuration

Manuscript received October 20, 2020; revised December 7, 2020; accepted December 12, 2020. Date of publication March 31, 2021; date of current version March 5, 2021.
* Corresponding Author, E-mail: yongli@hnu.edu.cn
* Supported by the Key Research and Development Program of Hunan Province of China (2018GK2031), National Natural Science Foundation of China (51822702), 111 Project of China (B17016), Innovative Construction Program of Hunan Province of China (2019RS1016) and China Scholarship Council (No. 201906130196).
Digital Object Identifier: 10.23919/CJEE.2021.000003

To realize the multiparallel operation of converters, droop control, which exhibits the parallel operation characteristics of synchronous generations, is proposed. It is noteworthy that several variants of droop control exist. To restore voltages and minimize voltage deviation, a coordinated droop control method using the virtual voltage axis, i.e., the voltage compensation term, was proposed in Ref. [6], and the effect of communication delay on the control effect was investigated. An adaptive droop control was proposed in Ref. [7] to overcome the nonlinear property of DC-MGs, and adaptive proportional integral (PI) controllers were introduced to adjust droop resistance and shift droop lines, which can remove the current-sharing deviation. A grid controller based on model predictive control for coordinating all droop controllers was designed in a previous study in Ref. [8] to minimize deviations in the DC voltages of the MTDC grid and avoid control mode changes. Ref. [9] proposed an adaptive droop control that included a voltage regulator generating a voltage correction term and a current regulator updating the droop coefficient. Refs. [10-11] used droop control to balance the state of charge (SOC) of each energy storage unit to avoid overusing a certain unit. The droop schemes above solved the problems of voltage deviation and unequal power sharing. However, they cannot provide sufficient damping and inertia for DC-MGs. High-frequency voltage resonance, voltage fluctuation, and voltage oscillation remain to be solved. In addition, a low-pass filter (LPF) is typically added to droop control to reduce the effects of measured harmonics. Furthermore, it was discovered that virtual inertia was unintentionally introduced into DC-MGs by LPFs.

To increase system damping and inertia simultaneously, virtual inertia and damping (VID) control was proposed through analogy with an AC system in Ref. [12]. However, the virtual inertia cannot be provided by the utility grid when the DC-MG is isolated. Hence, distributed ESSs with appropriate control methods are necessitated to stabilize the DC bus voltage and effectively eliminate voltage variations such that the inertia response of a DC system can be improved [13-14]. By simulating the external characteristics of DC machines, virtual DC machine control was proposed to improve the dynamic characteristics [15-16]. Emulating the charge and discharge characteristics of capacitors, virtual damping and inertia control were proposed in Ref. [17]. The difference in transient response between droop control and virtual synchronous generation control caused by the virtual inertia loop was investigated in Ref. [18]. An additional voltage-error mutual feedback control method was proposed to improve the stability of cascaded DC-DC converters in Ref. [19]. Ref. [20] investigated the insufficient inertia support in PV power-generation systems. The dynamic stability mechanisms of different virtual inertia controls have not been comprehensively analyzed and compared.

In this study, the dynamic stability mechanisms of droop+LPF control and virtual inertia control were investigated and compared to understand the differences in the damping improvement and inertia enhancement mechanism caused by LPF and virtual inertia loop. Simplified small-signal models were constructed, and the transfer function between different variables were derived to perform a theoretical analysis. To elaborate the dynamic stability of the abovementioned control methods, the effects of different control parameters on their eigenvalue distributions were analyzed. This provides a guideline for parameter design. Simulation results from Matlab verified the theoretical analysis. This study can facilitate studies in related research areas and the proposal of new control methods.

2 Investigated system and its conventional droop control

Fig. 2a shows a diagram of a single-bus DC-MG, which primarily included DGs, an ESS, and DC loads. The DGs were primarily composed of PVs, whereas the ESS was composed of batteries. The DC loads can be regarded as constant power loads (CPLs) because of the fast response and high bandwidth controller. The boost and buck circuits employed realize voltage conversions of DGs and DC loads, respectively, and they were connected to the DC bus via DC cables. The ESS was connected to the DC bus through a bidirectional DC (bi-DC) converter and a DC cable. L_s and R_s represent the filter inductance and its resistance, respectively; v_s and i_s represent the input voltage and input current, respectively; v_{out} and i_{out} represent the

output voltage and output current, respectively. DC voltage stabilization and multiparallel operation were realized through dual loop control (DLC) and droop control, as shown in Figs. 2b and 2c. $G_v(s)=k_{vp}+k_{vi}/s$ represents the voltage outer loop PI controller, and $G_i(s)=k_{ip}+k_{ii}/s$ the current inner loop PI controller. This study focused primarily on the control methods for the ESS and their effects on system dynamic stability. The droop control is expressed as shown in Eq. (1), where R_{droop} is the droop coefficient selected based on Eq. (2) and Fig. 2d.

$$v_{ref}=v_{dcn}-i_{out}\cdot R_{droop} \tag{1}$$

$$R_{droop}=\frac{\Delta v_{out\_max}}{\Delta i_{s\_max}}=\frac{v_{max}-v_{max}}{i_{o1\_max}-i_{o1\_min}} \tag{2}$$

where v_{max} and v_{min} are the maximum and minimum values of v_{out}, respectively. i_{o1_max} and i_{o1_min} are the maximum discharge current and maximum charge current of the ESS, respectively. v_{ref} is the reference value of v_{out}, and v_{dcn} is the rated value of v_{out}. As shown in Fig. 2d, each ESS can automatically allocate power based on their capacity. Hence, inappropriate operation modes, such as overcharge, overdischarge and SOC imbalance, can be avoided. Furthermore, the lifespan of the batteries can be extended.

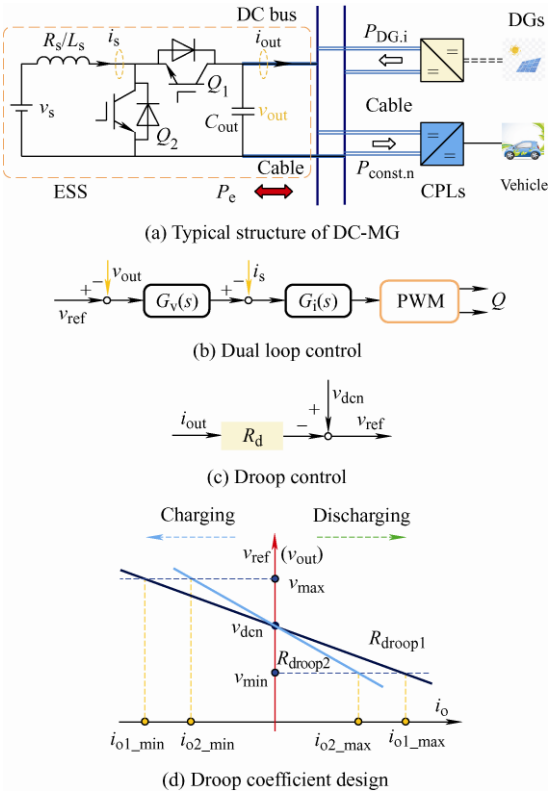

Fig. 2 Typical DC microgrid and its traditional control

The load converters are typically controlled using a fast-response and high bandwidth regulator. The negative impedance characteristic of the CPL reduces the stability margin and system damping. Hence, the DC-MG is a poor damping and low-inertia power system. The system and control parameters used are shown in Tab. 1 and Tab. 2.

Tab. 1 System parameters

Subsystem	Parameter	Value
DGs	Switching frequency f_s/kHz	10
	Input voltage v_s/V	100
	Inductor L_s/mH	5
	Resistance R_s/Ω	0.01
	Capacitor C_{out_DG}/μF	2 400
ESS	Switching frequency f_s/kHz	10
	Input voltage v_s/V	100
	Inductor L_s/mH	5
	Resistance R_s/Ω	0.01
	Capacitor C_{out}/μF	2 400
CPL	Switching frequency f_s/kHz	10
	Input voltage v_{in}/V	300
	Inductor L_s/mH	4
	Output capacitor C_{out}/μF	100
	Input capacitor C_{in}/μF	3 000
DC bus	DC cable L_{cable}(R_{cable})/mH(Ω)	0.1(0.01)
	DC bus capacitance C_{bus}/μF	3 000

Tab. 2 Control parameters

Control strategy	Parameter	Value
Droop control	Droop coefficient R_{droop}	2
	Voltage loop $k_{vp}+k_{vi}/s$	1+10
	Current loop $k_{ip}+k_{ii}/s$	5+1
	ω_c/(rad/s)	30
Virtual inertia and damping control	Inertia coefficient J_{vir}	0.06
	Damping coefficient D_{damp}	5
	Droop coefficient k_{droop}	0.5
	Voltage loop $k_{vp}+k_{vi}/s$	0.1+50

The passive network composed of DC cables and filter capacitors forms a resonance path, as shown in Fig. 3a, and may result in voltage resonance in the DC bus. Based on the parameters shown in Tab. 1, the transfer function of the passive network impedance is as shown in Eq. (3), and its impedance characteristics are shown in Fig. 3b. Resonance peaks appeared at frequencies 324 Hz and 428 Hz, indicating the risk of

resonance at these two frequencies. The resonant peak at 324 Hz was much higher than that at 428 Hz. Therefore, the resonance component near 324 Hz would be much higher than that at 428 Hz. When the system is disturbed, because the capacitance is insufficient to provide inertia, the DC voltage is prone to fluctuation and oscillation. The two problems above adversely affect the stability and operating efficiency of the DC-MG, thereby hindering its practical application.

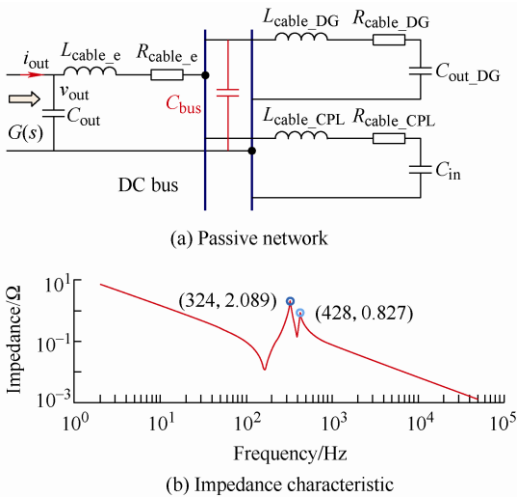

Fig. 3 Passive network and its impedance characteristic

$$\begin{cases} G(s)=\dfrac{1}{sC_{out}}\Big\|\left[(G_{DG}(s)\|G_{CPL}(s)\|\dfrac{1}{sC_{bus}})+(sL_{cable\_e}+R_{cable\_e})\right] \\ G_{DG}(s)=sL_{cable\_DG}+R_{cable\_DG}+\dfrac{1}{sC_{out\_DG}} \\ G_{CPL}(s)=sL_{cable\_CPL}+R_{cable\_CPL}+\dfrac{1}{sC_{out\_CPL}} \end{cases} \tag{3}$$

Many methods have been proposed to improve damping and solve the problem of insufficient inertia, of which the primary methods include active damping control and virtual inertia control. In this study, the damping improvement and inertia enhancement mechanism of droop+LPF control and VID control were investigated, and their dynamic stabilities were compared.

3 Virtual inertia control in DC-MG

This section provides a review of droop+LPF control and VID control. Both methods can increase the inertia of the DC-MG and improve the dynamic response of the DC voltage.

3.1 Droop+LPF control

To suppress resonance and reduce the effects of measured current harmonics, an LPF, expressed as $G_{lpf}(s)=\omega_c/(s+\omega_c)$, is typically added to the droop control loop. ω_c is the cutoff frequency of the LPF. Eq. (1) can be rewritten into the form of Eq. (4a), and $i_{ref}=0$. Fig. 4a shows an illustration of droop+LPF control. Generally, the bandwidth of the voltage-and-current dual loop is much higher than that of the LPF. Therefore, Eq. (4a) can be rewritten as Eq. (4b). Based on Eq. (4), adding an LPF introduces virtual inertia to a DC-MG, and this effect is similar to the virtual inertia presented in Ref. [12]. To understand the effect of virtual inertia more comprehensively and compare the effects of virtual inertia provided by different control methods, a review of VID control is provided next.

$$\begin{cases} \dfrac{s}{R_{droop}\omega_c}(v_{ref}-v_{dcn})=i_{ref}-i_{out}-\dfrac{1}{R_{droop}}(v_{ref}-v_{dcn}) & (4a) \\ \dfrac{s}{R_{droop}\omega_c}(v_{out}-v_{dcn})=i_{ref}-i_{out}-\dfrac{1}{R_{droop}}(v_{out}-v_{dcn}) & (4b) \end{cases}$$

3.2 VID control

Typically, a DC capacitor can alleviate DC voltage fluctuation by absorbing or supporting energy when power imbalance occurs in a DC-MG, as shown in Eq. (5a). However, the inherent inertia of capacitors is extremely small; as such, a DC-MG is typically a low-inertia system without sufficient ability to suppress voltage fluctuation completely.

To solve the problem of insufficient inertia, the concept of virtual inertia is proposed. By emulating the charging and discharging process of the capacitor, the external characteristics of the converter can be regulated to enhance the system inertia and smooth the DC voltage fluctuation. Therefore, virtual inertia is equivalent to paralleling a large virtual capacitor $C_{vir}(=J_{vir})$ on the output side of the converter. Under the same power disturbance, the fluctuation range and change rate of the DC voltage are effectively limited by C_{vir}, as shown in Eq. (5b). Under the action of droop control, the DC voltage typically changes around its rated value v_{dcn}. To prevent the inertia loop from affecting the DC voltage regulation and power sharing, v_{dcn} is added into the virtual inertia loop to obtain a better dynamic performance, as shown in Eq. (5b), where i_{in} refers to the reference value of i_{out}.

$$\begin{cases} i_{\text{in}} - i_{\text{out}} = C_{\text{out}} \dfrac{\mathrm{d}v_{\text{out}}}{\mathrm{d}t} = C_{\text{out}} \dfrac{\mathrm{d}(v_{\text{out}} - v_{\text{dcn}})}{\mathrm{d}t} & (5a) \\ i_{\text{in}} - i_{\text{out}} = (C_{\text{out}} + C_{\text{vir}}) \dfrac{\mathrm{d}(v_{\text{out}} - v_{\text{dcn}})}{\mathrm{d}t} & (5b) \end{cases}$$

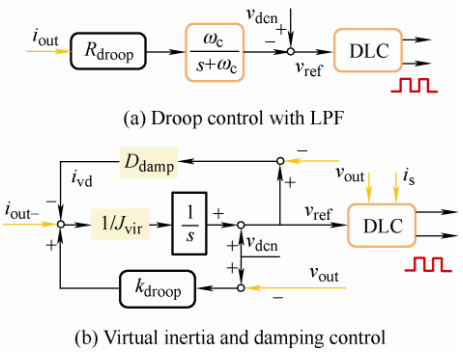

Fig. 4 Two typical control methods of bi-DC converter

Additionally, an active damping loop is introduced to solve the negative damping caused by the CPL and improve the system damping. The damping current is calculated using Eq. (6). The damping current changes with v_{out}, and it will be 0 when v_{out} is equivalent to its reference v_{ref}.

$$i_{\text{vd}} = D_{\text{damp}} (v_{\text{ref}} - v_{\text{out}}) \quad (6)$$

Combining the droop control presented in Eqs. (5) and (6), the VID control equation can be obtained, as shown in Eq. (7). The block diagram of VID control, as shown in Fig. 4b, includes a voltage and current DLC, a VID loop, and droop control. The VID loop provide inertia and damping to the DC-MG and generates v_{ref}. Under the action of DLC, v_{ref} can be tracked by v_{out}, thereby eliminating steady-state errors

$$sC_{\text{vir}} (v_{\text{out}} - v_{\text{dcn}}) = \frac{1}{R_{\text{droop}}} (v_{\text{dcn}} - v_{\text{out}}) - i_{\text{out}} - D_{\text{damp}} (v_{\text{ref}} - v_{\text{out}}) \quad (7)$$

As shown in Eqs. (4b) and (6), droop+LPF control is essentially the same as VID control. The virtual inertia of VID is contributed by the virtual capacitors C_{vir}, and the inertia of droop+LPF control is controlled by ω_c and R_{droop}, as shown in Eq. (8). The damping of VID control is provided by R_{droop} and D_{damp}, and the damping of droop+LPF control is affected by R_{droop}. Generally, R_{droop} is not adjustable, whereas D_{damp} can be adjusted within a certain range. Therefore, droop+LPF control might not provide sufficient damping.

$$\frac{1}{R_{\text{droop}} \omega_c} = C_{\text{vir}} \quad (8)$$

3.3 Small-signal model

The following equation can be derived from the power balance by disregarding the power loss of the bi-DC converter

$$V_s \Delta i_s = (I_{\text{out}} + s \cdot 2 \cdot C_{\text{out}} V_{\text{out}}) \cdot \Delta v_{\text{out}} + V_{\text{out}} \Delta i_{\text{out}} \quad (9)$$

Therefore, the relationship between the output current i_{out} and input current i_s can be obtained, as follows

$$G_{\text{ii}} = \frac{\Delta i_{\text{out}}}{\Delta i_s} = \frac{V_s}{V_{\text{out}}} \quad (10)$$

Using the state space equation of bi-DC converters, the transfer function between the input current i_s and duty cycle d can be obtained.

$$G_{\text{id}} = \frac{\Delta i_s}{\Delta d} = \frac{C_{\text{out}} V_{\text{out}} s + (1-D) I_s}{L_s C_{\text{out}} s^2 + R_s C_{\text{out}} s + (1-D)^2} \quad (11)$$

Combining Eqs. (10) and (11), the small-signal model of droop+LPF control can be derived, as shown in Fig. 5a. The transfer function $TF_{\text{v\_d}}(s)$ between Δv_{out} and Δv_{dcn} is shown in Eq. (12), and its closed-loop output impedance $Z_{\text{out\_droop}}(s)$ is shown in Eq. (13). R'_{droop} is the redefined droop coefficient, which is further defined as shown in Eq. (14). k_{pwm} is the gain of PWM modulation.

$$TF_{\text{v\_d}} = \frac{\Delta v_{\text{out}}}{\Delta v_{\text{dcn}}} = \frac{G_{\text{v}} \cdot G_{\text{i}} \cdot k_{\text{pwm}} \cdot G_{\text{id}} \cdot G_{\text{ii}} \cdot Z_{\text{net}}}{1 + G_{\text{i}} k_{\text{pwm}} G_{\text{id}} + G_{\text{v}} G_{\text{i}} k_{\text{pwm}} G_{\text{id}} R'_{\text{droop}} G_{\text{ii}} + G_{\text{v}} G_{\text{i}} k_{\text{pwm}} G_{\text{id}} G_{\text{ii}} \cdot Z_{\text{net}}} \quad (12)$$

$$TF_{\text{i\_d}} = \frac{\Delta v_{\text{out}}}{\Delta i_{\text{out}}} = \frac{-G_{\text{v}} \cdot G_{\text{i}} \cdot k_{\text{pwm}} \cdot G_{\text{id}} \cdot G_{\text{ii}} \cdot Z_{\text{net}} R'_{\text{droop}}}{1 + G_{\text{i}} k_{\text{pwm}} G_{\text{id}} + G_{\text{v}} G_{\text{i}} k_{\text{pwm}} G_{\text{id}} G_{\text{ii}} \cdot Z_{\text{net}}} = -Z_{\text{out\_droop}} \quad (13)$$

$$R'_{\text{droop}} = \begin{cases} R_{\text{droop}} & \text{Droop control} \\ R_{\text{droop}} G_{\text{lpf}} & \text{Droop + filter} \end{cases} \quad (14)$$

Combining Eq. (10), Eq. (11), and Fig. 4b, the small-signal model of VID control is as shown in Fig. 5b. The transfer function $TF_{\text{v\_id}}(s)$ between Δv_{out} and Δv_{dcn} is shown in Eq. (15a). Its closed-loop output impedance $Z_{\text{outcl}}(s)$ is expressed in Eq. (15b).

$$\begin{cases} TF_{\text{v\_id}} = \dfrac{\Delta v_{\text{out}}}{\Delta v_{\text{dcn}}} = \dfrac{\left(k_{\text{droop}} + s \cdot J_{\text{vir}}\right) \cdot G_{\text{v}} \cdot G_{\text{ii}} \cdot Z_{\text{net}}}{sJ_{\text{vir}}\left(1 + G_{\text{v}} G_{\text{ii}} Z_{\text{net}}\right) + D_{\text{damp}} + G_{\text{v}} G_{\text{ii}} + k_{\text{droop}} G_{\text{v}} G_{\text{ii}} \cdot Z_{\text{net}}} & (15a) \\ TF_{\text{i\_id}} = \dfrac{\Delta v_{\text{out}}}{\Delta i_{\text{out}}} = \dfrac{-G_{\text{v}} \cdot G_{\text{ii}} \cdot Z_{\text{net}}}{sJ_{\text{vir}} + D_{\text{damp}} + G_{\text{v}} G_{\text{ii}} Z_{\text{net}}\left(k_{\text{droop}} + sJ_{\text{vir}}\right)} = -Z_{\text{outcl}} & (15b) \end{cases}$$

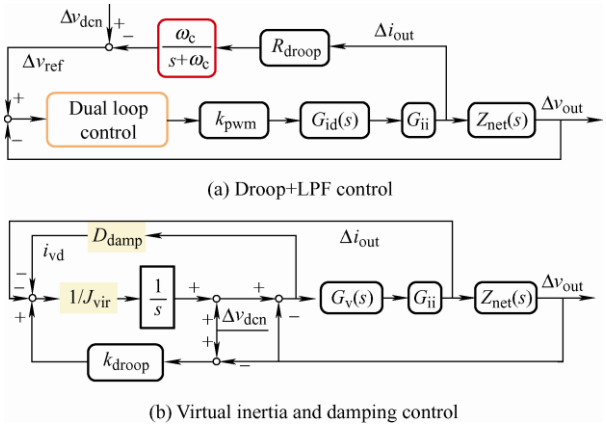

Fig. 5 Small-signal model of DC-MG with different control methods

4 Transient stability analysis

To observe the transient stability of the DC voltage when the ESS regulates the bus voltage using different control methods, eigenvalues analyses were performed, the results of which are shown in Fig. 6 and Fig. 7.

The dominant eigenvalue distribution diagram of droop control and droop+LPF control is presented in Fig. 6. As shown in Fig. 6, the DC-MG can be simplified to a third-order system. The dominant eigenvalues comprise a negative real root and a pair of conjugate negative complex roots. The negative real root dominates the inertia component, whereas the conjugate complex root controls the oscillation mode.

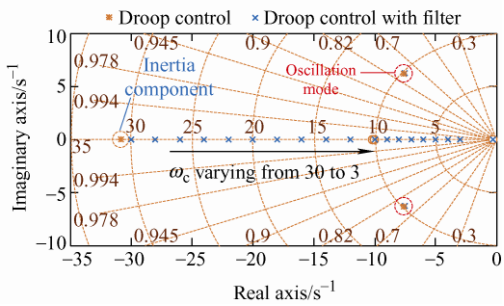

Fig. 6 Eigenvalue distribution of droop control w/wo LPF

When the LPF is not considered, all the eigenvalues of droop control are constant in the circle. The inertia component and oscillation mode cannot be regulated by droop control. Therefore, when the system is disturbed, the DC voltage would fluctuate or oscillate. Considering the LPF, the negative real root moves toward the imaginary axis, whereas the conjugate complex root remains stationary.

As shown in Fig. 6, the LPF affects the position of the negative real root. ω_{c} can change the time constant of the inertia component and the voltage change rate, but it cannot affect the oscillation mode. Therefore, although droop+LPF control introduces virtual inertia to the DC-MG, it cannot improve the damping that suppresses the oscillation mode. Furthermore, the DC voltage contains an oscillation component during the transient process.

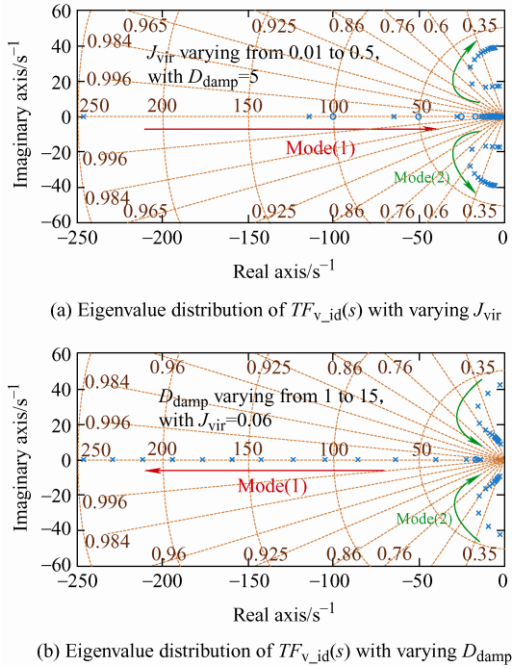

Fig. 7 Eigenvalue distribution of VID control

The eigenvalue distribution of $TF_{\text{v\_id}}(s)$ is shown in Fig. 7. Similar to droop control, the DC-MG with VID control can still be simplified to a third-order system, including a negative real root and a pair of negative conjugate complex roots. However, the positions of the three dominant roots are affected by the control parameters J_{vir} and D_{damp}. As shown in Fig. 7a, the negative real root moves

toward the imaginary axis gradually as J_{vir} increased. Hence, the time constant of the inertia component and the system inertia increased gradually. The damping of the oscillation mode increased gradually at first and then decreased as J_{vir} increased. The oscillation frequency increased gradually as J_{vir} increased.

As shown in Fig. 7b, the negative real root moves away from the imaginary axis gradually as D_{damp} increased, indicating that the inertia decreased gradually. The change rate of the DC voltage increased gradually, whereas the time constant of the inertia component decreased. Furthermore, with the increase in D_{damp}, the damping of the oscillation mode increased at first and then decreased. The oscillation frequency is negatively correlated with D_{damp}. Therefore, to obtain a better control performance, J_{vir} and D_{damp} should not be larger to limit the rate of change of the DC voltage and suppress voltage oscillation effectively. To summarize, droop control cannot provide virtual inertia and damping to the DC-MG. Applying an LPF introduces virtual inertia to the DC-MG unintentionally, and the droop resistance can provide active damping. The virtual inertia is affected by the filter bandwidth, i.e., ω_c, and the droop coefficient is limited by the voltage deviation; therefore, the active damping is not adjustable. Virtual inertia and damping control provide flexible and adjustable virtual inertia as well as active damping to the DC-MG. By setting the appropriate J_{vir} and D_{damp} values, virtual inertia and active damping can be adjusted. A comparison of the control performance is shown in Tab. 3.

Tab. 3 Control performance comparison

Control strategy	Inertia	Damping
Droop control	No	No
Droop+LPF control	Yes	Yes, but non-adjustable
Virtual inertia and damping control	Yes	Yes, and adjustable

5 Simulation results

Based on Fig. 2 and the parameters listed in Tab. 1 and Tab. 2, a DC-MG model was established in Matlab to validate the theoretical analysis performed in this study. The power disturbance was replaced by the step change of the CPL. The load power was increased by 500 W at 3 s and decreased by 500 W at 6 s. The simulation results are shown in Figs. 8 and 9.

Under droop control, the DC-MG could not provide sufficient damping to suppress high-frequency resonance, and the CPL exhibited negative damping characteristics, thereby resulting in high-frequency resonance in the DC bus voltage. The simulation result is shown in Fig. 8a. The fast Fourier transform (FFT) of the output voltage and output current are shown in Figs. 8b and 8c, respectively. As shown in these figures, the resonance component at 323 Hz was much higher than that at 426 Hz, which is consistent with the analysis shown in Fig. 3. In addition, when the DC-MG was disturbed, the DC voltage indicated significant voltage fluctuation and oscillation.

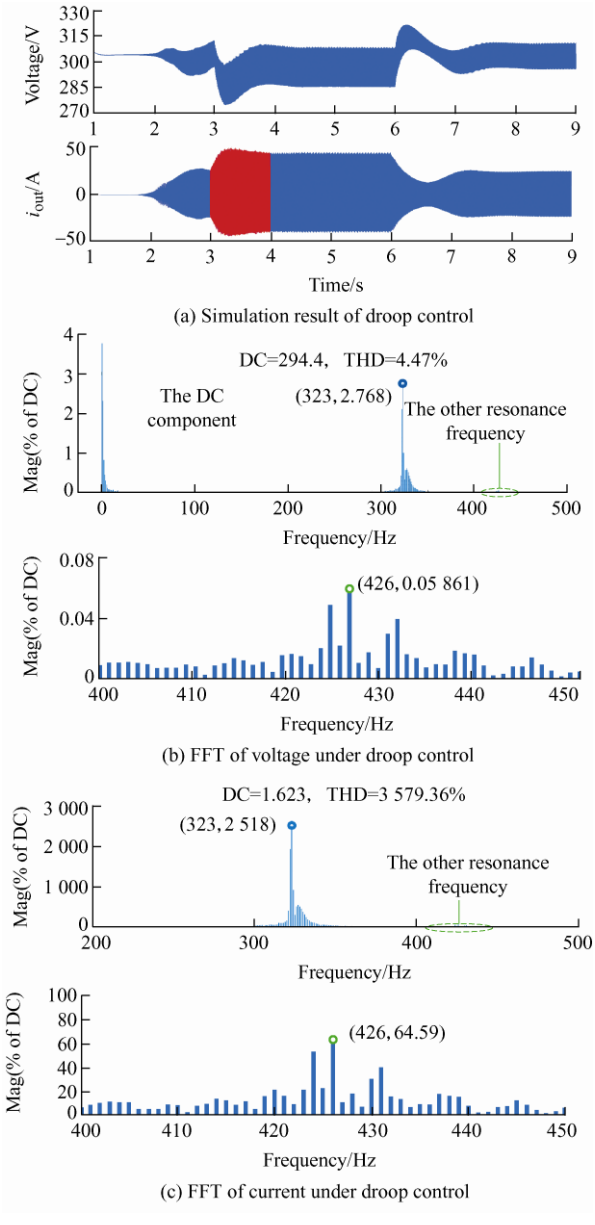

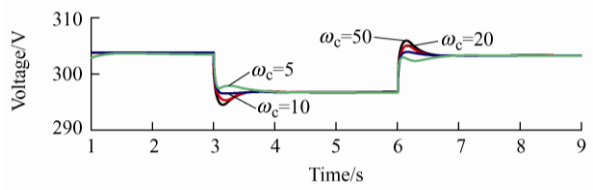

(d) Simulation result of droop+LPF control

Fig. 8 Simulation of droop control and droop+LPF control

To reduce the effects of high-frequency harmonics, an LPF $G_{lpf}(s)$ is typically added in the droop control loop. The simulation result is shown in Fig. 8d. As shown, high-frequency resonance was effectively suppressed because of $G_{lpf}(s)$. With the decrease in ω_c, the change rate of the DC voltage decreased, indicating that the inertia of the DC-MG was increasing gradually. However, an oscillation component remained in the transient process, and it was barely affected by ω_c. The simulation results are consistent with the analysis shown in Fig. 6.

The simulation results of VID control are presented in Fig. 9. As shown, the transient voltage was primarily composed of a first-order component and an oscillation component. Based on Fig. 9a, the first-order component required more time to transition to the steady state as J_{vir} increased gradually. Simultaneously, the oscillation frequency increased gradually, whereas the oscillation amplitude decreased at first and then increased, implying that the system damping increased at first and then decreased. As shown in Fig. 9b, as D_{damp} increased, the oscillation frequency decreased gradually, and the damping increased at first and then decreased. The analysis above shows that J_{vir} and D_{damp} should not be excessively large. The simulation results were consistent with the analysis results shown in Fig. 9. In summary, VID control can increase damping and enhance inertia, thereby attenuating resonance and improving the transient response.

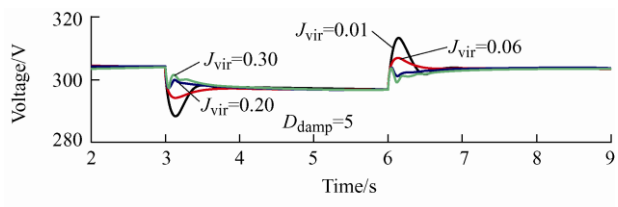

(a) Simulation result with varying J_{vir}

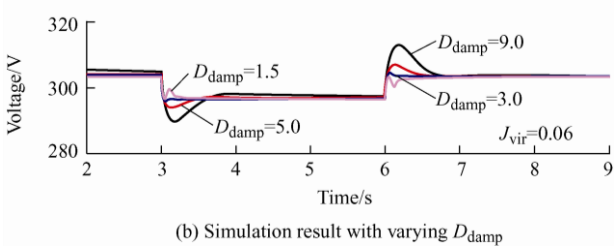

(b) Simulation result with varying D_{damp}

Fig. 9 Simulation results of VID control

The analysis above shows that droop+LPF control can only provide inertia to the DC-MG to reduce the voltage change rate of the inertia component; it does not increase the damping to suppress the amplitude oscillation mode. Meanwhile, VID control can improve the inertia and damping simultaneously. The change rate of the inertia component can be reduced by increasing J_{vir}. Meanwhile, the damping of the oscillation mode can be increased by selecting an appropriate D_{damp}; hence, its amplitude can be reduced. Compared with droop+LPF control, VID control possesses an additional degree of freedom; hence, it affords a more flexible control.

6 Conclusions

In this study, small-signal models of droop control, droop+LPF control, and VID control were established to compare the dynamic stabilities of these three control methods. Based on eigenvalue analysis, the DC-MG is equivalent to a third-order system. Subsequently, the mechanisms of both inertia and damping enhancements were analyzed. The theoretical analysis results were verified via simulation. The conclusions obtained were as follows.

(1) Compared with droop control, droop+filter control and VID control can suppress high-frequency resonance and damp voltage oscillation more effectively.

(2) Based on eigenvalue analysis, the LPF introduced virtual inertia to the DC-MG, and the voltage change rate can be controlled by ω_c. However, because it did not affect the oscillation mode, the voltage oscillation could not be damped.

(3) Based on eigenvalue analysis, VID control can provide both inertia and damping. Virtual inertia and oscillation frequency are positively

correlated with J_{vir} and negatively correlated with D_{damp}. To ensure that voltage oscillation is suppressed, J_{vir} and D_{damp} should not be set to excessively large values.

(4) Droop+LPF control cannot provide damping to the oscillation mode, whereas VID control can provide both inertia and damping. Therefore, droop+LPF control and VID control can be used in scenarios not requiring and requiring better voltage quality, respectively.

References

[1] M Yang, Y W Wu, Y Z Zhu, et al. Coordinated control for autonomous DC microgrid with dynamic load power sharing. *Power System Technology*, 2017, 41(2): 440-447.

[2] X Y Wang, G F Tang, X G Wei, et al. LCL-based resonant modular multilevel DC/DC converter for DC grids. *Power System Technology*, 2017, 41(4): 1106-1113.

[3] G Lin, Y Li, Z Y Wang, et al. Resonance mechanism analysis and its active damping suppression of LVDC distribution system. *Power System Technology*, 2017, 41(10): 3358-3364.

[4] M S Wang, Z M Li, Y Wang. Distribution network distributed power supply configuration considering the uncertainties of electric vehicle. *Power System Protection and Control*, 2019, 47(1): 67-72.

[5] S Cheng, S Y Wu, W B Sun. Optimal planning of charging stations for electric vehicles considering voltage stability of distribution system and the quality of service. *Power System Protection and Control*, 2019, 47(7): 12-21.

[6] B Ko, G Lee, K Choi, et al. A coordinated droop control method using a virtual voltage axis for power management and voltage restoration of DC microgrids. *IEEE Transactions on Industrial Electronics*, 2018, 66(11): 9076-9085.

[7] M Mokhtar, M I Marei, A A El-Sattar. An adaptive droop control scheme for DC microgrids integrating sliding mode voltage and current controlled boost converters. *IEEE Transactions on Smart Grid*, 2019, 10(2): 1685-1693.

[8] G Li, Z Du, C Shen, et al. Coordinated design of droop control in MTDC grid based on model predictive control. *IEEE Transactions on Power Systems*, 2018, 33(3): 2816-2828.

[9] V Nasirian, A Davoudi, F L Lewis, et al. Distributed adaptive droop control for DC distribution systems. *IEEE Transactions on Energy Conversion*, 2014, 29(4): 944-956.

[10] X Lu, K Sun, J M Guerrero, et al. State-of-charge balance using adaptive droop control for distributed energy storage systems in DC microgrid applications. *IEEE Transactions on Industrial Electronics*, 2014, 61(6): 2804-2815.

[11] X Lu, K Sun, J M Guerrero, et al. Double-quadrant state-of-charge-based droop control method for distributed energy storage systems in autonomous DC microgrids. *IEEE Transactions on Smart Grid*, 2015, 6(1): 147-157.

[12] W Wu, Y Chen, A Luo, et al. A virtual inertia control strategy for DC microgrids analogized with virtual synchronous machines. *IEEE Transactions on Industrial Electronics*, 2017, 64(7): 6005-6016.

[13] Y Li, L He, F Liu, et al. Flexible voltage control strategy considering distributed energy storages for DC distribution network. *IEEE Transactions on Smart Grid*, 2019, 10(1): 163-172.

[14] X Zhu, Z Xie, S Jing, et al. Distributed virtual inertia control and stability analysis of DC microgrid. *IET Generation, Transmission & Distribution*, 2018, 12(14): 3477-3486.

[15] S Samanta, J P Mishra, B K Roy. Virtual DC machine: An inertia emulation and control technique for a bidirectional DC-DC converter in a DC microgrid. *IET Electric Power Applications*, 2018, 12(6): 874-884.

[16] G. Lin, J Ma, Y Li, et al. A virtual inertia and damping control to suppress voltage oscillation in islanded DC microgrid. *IEEE Transactions on Energy Conversion*, DOI: 10.1109/TEC.2020.3039364.

[17] X Zhu, F Meng, Z Xie, et al. An inertia and damping control method of DC-DC converter in DC microgrids. *IEEE Transactions on Energy Conversion*, 2020, 35(2): 799-807.

[18] J Liu, Y Miura, T Ise. Comparison of dynamic characteristics between virtual synchronous generator and droop control in inverter-based distributed generators. *IEEE Transactions on Power Electronics*, 2016, 31(5): 3600-3611.

[19] Z Guo, H Li, C Liu, et al. Stability-improvement method of cascaded DC-DC converters with additional voltage-error mutual feedback control. *Chinese Journal of Electrical Engineering*, 2019, 5(2): 63-71.

[20] X Zhang, Q Gao, Y Hu, et al. Active power reserve photovoltaic virtual synchronization control technology. *Chinese Journal of Electrical Engineering*, 2020, 6(2): 1-6.

Gang Lin received the B.S. degree in electrical engineering and automation from Guizhou University, Guiyang, China, in 2016, and the M.S. degree in electrical engineering from the Hunan University, Changsha, China, in 2019. He is currently pursuing the Ph.D. degree in electrical engineering at TU Dortmund University, Dortmund, Germany.

Since 2019, he has been a research associate with Institute of Energy Systems, Energy Efficiency and Energy Economics, TU Dortmund University. His current research interests include stability analysis, virtual inertia control, and integrated energy system.

Wei Zuo received the B.S. degree in electrical engineering and automation from University of South China, Hengyang, China, in 2018, and the M.S. degree in electrical engineering from the Hunan University, Changsha, China, in 2020. She is currently pursuing the Ph.D. degree in electrical engineering at University of Leeds, Leeds, UK.

Her current research interests include traction power system reliability analysis, equipment fault analysis, and system reliability allocation.

Yong Li (S'09-M'12-SM'14) was born in Henan, China, in 1982. He received the B.S. and Ph.D. degrees in 2004 and 2011, respectively, from the College of Electrical and Information Engineering, Hunan University, Changsha, China. Since 2009, he worked as a research associate at the Institute of Energy Systems, Energy Efficiency, and Energy Economics (IE3), TU Dortmund University, Dortmund, Germany, where he received the second Ph.D. degree in June 2012.

He is currently a full professor of electrical engineering with Hunan University. His research interests include power system stability analysis and control, ac/dc energy conversion systems and equipment, analysis and control of power quality, and HVDC and FACTS technologies.

Jiayan Liu (S'20) received the B.S. degree in electrical engineering and automation from Northwest A&F University, Yangling, China, in 2016, and the M.S. degree in electrical engineering from the Hunan University, Changsha, China, in 2018. He is currently pursuing the Ph.D. degree in electrical engineering at TU Dortmund University, Dortmund, Germany.

Since 2018, he has been a research associate with Institute of Energy Systems, Energy Efficiency and Energy Economics, TU Dortmund University. His current research interests include electric vehicle charging scheduling, resource allocation, smart grid, and integrated energy system.

Shaoyang Wang was born in Hebei, China, in 1994. He received the B.S. degree in automation from the Changsha University of Science and Technology, Changsha, China, in 2017, and the M.S. degree in electrical engineering in 2019 from Hunan University, Changsha, China, where he is currently working toward the Ph.D. degree with the College of Electrical and Information Engineering. His research interest is power quality analyses and control.

Pengcheng Wang received the B.S. degree in electrical engineering and automation from Central South University, Changsha, China, in 2016, and the M.S. degree in electrical engineering from Hunan University, Changsha, China, in 2019. He is currently pursuing the Ph.D. degree in the College of Electrical Engineering at Zhejiang University. His current research interests include modeling and stability analysis of power electronics-based power system, and microgrid.